water

MDPI

Article

CO_2 Viscosification for Mobility Alteration in Improved Oil Recovery and CO_2 Sequestration

Ali Zidane

Now with LRST at the National Energy Technology Laboratory, Morgantown, WV 26505, USA; ali.zidane@live.com

Abstract: Recently there have been significant advances in the viscosification of CO_2 using a low concentration of oligomers. The new engineered molecules do not adsorb onto rock. This paper studies the effects of different CO_2-enhanced viscosity levels in subsurface aquifers and reservoirs. The study was conducted using numerical modeling and simulation tools in homogeneous, heterogenous, fractured, and unfractured media. The viscosity enhancement of CO_2 varied from 2- to 20-fold. The simulations included homogeneous, layered, and fractured domains in 2D and in 3D for improved oil recovery. The results showed that in unfractured, homogenous, and layered media, a 10-fold viscosity increase leads to significant increases in oil recovery. In a fractured medium with a highly connected fracture network, a 20-fold viscosity enhancement may have a considerable effect in delaying breakthrough and improving oil recovery. Simulations were performed in a compositional three-phase flow based on higher-order discretization. The algorithm included Fickian diffusion, which may add to oil recovery performance when there is a sufficient surface area between the CO_2-rich phase and the oil phase. In CO_2 sequestration, an increase in the viscosity of CO_2 and consequent mobility control promotes CO_2 dissolution in the aqueous phase. Due to the increase in the density of the aqueous phase from CO_2 dissolution, the CO_2 is carried away from the cap rock to the bottom of the formation. This work is of particular importance in improved oil recovery and in safe CO_2 sequestration due to solubility trapping and mitigation of pressure increase. The higher-order numerical scheme used in this simulation guarantees a level of accuracy not obtained in traditional simulators.

Keywords: CO_2 mobility control; IOR; CO_2 sequestration; compositional flow

Citation: Zidane, A. CO_2 Viscosification for Mobility Alteration in Improved Oil Recovery and CO_2 Sequestration. *Water* **2023**, *15*, 1730. https://doi.org/10.3390/w15091730

Academic Editor: Chengyun Zhou

Received: 3 March 2023
Revised: 24 April 2023
Accepted: 27 April 2023
Published: 29 April 2023

1. Introduction

CO_2 emission to the atmosphere from fixed sources of production such as power, cement, aluminum, and steel plants and from oil and gas production constitutes more than one third of total emissions. Permanent storage of such a large amount of CO_2 in the subsurface may contribute greatly to the mitigation of global warming. A large amount of emitted CO_2 can be stored in subsurface brine aquifers. Large amounts of CO_2 can also be used in improved oil recovery, if it can be viscosified. The viscosification of CO_2 can be achieved using a low concentration of functional polymers. Lemaire et al. [1] showed that CO_2-soluble polymers with low molecular weights and oligomers could be considered as modest thickeners.

CO_2 has many desirable characteristics in improved oil recovery, both in secondary and tertiary modes. It swells the oil that it encounters, sometimes by as much as 80%. Swelling may be pronounced in both light oils and heavy oils. The method often has low residual oil saturation, which implies high microscopic displacement efficiency. It reduces the oil viscosity via dissolution, sometimes by an order of magnitude or more in heavier oils. The main drawback in the widespread use of CO_2 for IOR is very low viscosity, which results in low sweep efficiency and early breakthrough. CO_2 is a unique substance.

At subsurface conditions it is often a supercritical fluid which has gas-like viscosity and liquid-like density.

Mobility modification of injected fluids often enhances recovery in oil and gas production [2–4]. A viscosity reducer could be added to ease the displacement of the oil as shown in [2], whereas a viscosity thickener might be needed in cases of high mobility of the injected fluid. Water alternating gas (WAG) injection is one of the techniques used to improve sweep efficiency and increase oil recovery. Residual oil saturation from CO_2 displacement is usually less than that from water displacement. Alternating injections of water and CO_2 at different cycles are of interest in WAG injection because this process improves sweep efficiency with intermittent injections of water and CO_2 [5]. CO_2 swells the oil and reduces the oil's residual saturation more than other gases. In addition to the economic advantages of using CO_2 in WAG processes, it also has environmental benefits related to global warming because it reduces the amount of greenhouse gas emissions to the atmosphere.

CO_2 foam is another mobility control alternative [6,7]. A drawback of CO_2 injection is low sweep efficiency due to gravity override and/or viscous fingering induced by its high mobility with respect to the oil in place. To overcome this limitation, Bond and Holbrook [8] and Fried [9] have proposed the foam process in order to improve sweep efficiency for gas displacement processes. Despite the reduction in CO_2 mobility, different studies have shown that oil recovery is sometimes impaired [10] in CO_2 foam. Khulman [11] has shown that oil may destabilize foam by spreading at bubble/film interfaces. Other studies [12,13] have shown that partitioning of a surfactant into oil affects foam stability. There may be significant adsorption of the foam-forming surfactant on the rock. In addition, high-permeability channels could be plugged by the foam [14].

CO_2 viscosification is a viable alternative that takes advantage of CO_2 injection benefits and avoids the complexities of the foam process. CO_2 polymer thickeners have been proposed and recognized as a 'game-changing technology' [15] in oil recovery. A CO_2 thickener increases the viscosity, which leads to a mobility reduction of the injected CO_2. The main characteristics of an effective CO_2 thickener are low or negligible adsorption to rock, low partitioning in the oil phase and the aqueous phase, and reversibility in flow rate increases and decreases [16]. There are three different alternatives for CO_2 thickening: polymers and cosolvents, nanoparticles with and without polymers, and polymers alone. Bae and Irani [17] presented a CO_2 polymer thickener that increases CO_2 viscosity up to 90-fold with a cosolvent. At 6 wt% polymer concentration, the increase in viscosity is 3.5 cp, and a 2 wt% polymer increases it to 0.8 cp in reservoir conditions [17]. Despite the improved oil recovery in the core flow, the concentration of toluene cosolvent (up to 20 wt% toluene with 4 wt% polymer) makes the cost of field scale prohibitive. Nanoparticles have also been suggested for the vicosification of CO_2. Often the concentration is around 5 to 6 wt% for a five- to six-fold viscosity increase of CO_2 [16]. Use of a polymer additive such as a fluorinated compound may increase CO_2 viscosity by 4- to 20-fold in 1 wt% and higher concentrations [18–20]. However, the cost and environmental concern associated with fluorinated compounds are major limitations. CO_2 viscosification with direct thickeners in CO_2 emulsions in oil has been reviewed and validated experimentally in [1].The guidelines of engineering a new CO_2 viscosifier were established in [21]. The work presented in this paper is based on our recent findings on CO_2 viscosification and the engineering of new effective molecules. A five-fold viscosity enhancement has been shown to increase oil recovery in [16], but the breakthrough time remains the same with neat CO_2.

The presented study is concerned with the investigation of the extent of viscosification of CO_2 in field scale using numerical modeling and simulation tools. The study covers different domains with different levels of complexity varying from a homogeneous 2D domain to a fractured 3D domain. Different papers have studied the effect of CO_2-enhanced viscosity as in [16], however the work in [16] is based on a finite-difference scheme and is limited to unfractured media. The work presented in this paper overcomes the limitations of the finite-difference method by using higher-order discretization in the modeling approach.

The higher-order method provides a better description of physics with higher accuracy, in addition to ease of implementation in complex reservoirs. Numerical simulation results in this work show that CO_2-enhanced viscosity may significantly increase pressure mitigation and solubility trapping in CO_2 sequestration. The effect of different levels of viscosification is discussed in further detail in the following sections.

The paper is organized as follows: a general description of the model and the differential equations describing flow in unfractured and fractured porous media is presented in the first section; then, four numerical examples and a sensitivity study are discussed to demonstrate the effect of CO_2-enhanced viscosity in different porous media; concluding remarks are presented in the last section.

2. Method Description

The essence of our numerical solution is briefly outlined below:

- The traces of the pressure were implicitly calculated at the interfaces of grid-cells and matrix and fracture elements.
- The pressure at the grid-cells was updated using the calculated pressure at the interfaces.
- The total fluxes in the whole domain (between the grid-cells and matrix and fracture network) were evaluated by the mixed finite elements (MFE).
- The molar densities were evaluated using the discontinuous Galerkin (DG) method in unfractured media and in the matrix elements and the finite volume (FV) method in the fracture elements.
- The miscibility of CO_2 is a critical parameter when describing the flow behavior. In the model presented in this paper, the description of the miscibility depends on the existing components. As a result, two different equations of states were used based on the available components in the mixture.
- Phase-split calculations were performed in all grid-cells (including matrix and fracture) based on an initial guess from the stability analysis. In grid-cells where the water phase was absent, the Peng–Robinson [22] equation of state (EOS) was used. If the water phase was present, a cubic-plus-association (CPA) EOS was used [23].
- A multicomponent diffusion model [24] was used to calculate the diffusive fluxes. The formulation used in this work is based on the chemical potential gradient. The diffusive flux for a component i in phase α is given as follows:

$$J_{i,\alpha} = -\frac{\phi S_\alpha c_\alpha}{RT}\left(\sum_j x_{j,\alpha}\nabla\mu_{j,\alpha}{B_{i,j,\alpha}}^{-1}\right) \tag{1}$$

In the above equation, R is the gas constant, T is the temperature, $\mu_{j,\alpha}$ is the chemical potential of component j in phase α, and B is a matrix derived from the Stefan–Maxwell diffusion coefficients.

- The above methods have been discussed in several publications [25–30].

3. Governing Equations

For the sake of completeness, the main equations that govern the compositional two-and three-phase flow are presented.

The mass transport equations for component i in n_c-component mixture in the three-phase are given by:

$$\phi\frac{\partial cz_i}{\partial t} + \nabla.\left(\sum_\alpha c_\alpha x_{i,\alpha} v_\alpha + S_\alpha J_{i,\alpha}\right) = F_i, \quad i = 1..n_c \text{ in } \Omega \times (0,\tau) \tag{2}$$

and

$$\sum_{i=1}^{n_c} z_i = 1 \tag{3}$$

where ϕ denotes the porosity, v_α the velocity of phase α, c the overall molar density of the mixture, and z_i and F_i are the overall mole fraction and the sink/source term of component i in the mixture, respectively. c_α is the molar density of phase α, $x_{i,\alpha}$ is the mole fraction of component i in phase α, and $\boldsymbol{J_{i,\alpha}}$ is the diffusive flux of component i in phase α [25]. Ω is the computational domain, τ denotes the simulation time, and n_c is the number of components.

The velocity of phase α is given by Darcy's law:

$$\boldsymbol{v}_\alpha = -\frac{\boldsymbol{K}k_{r\alpha}}{\mu_\alpha}(\nabla p_\alpha - \rho_\alpha \boldsymbol{g}) = -\lambda_\alpha \boldsymbol{K}(\nabla p_\alpha - \rho_\alpha \boldsymbol{g}), \quad \alpha = g, o, w \tag{4}$$

where $\boldsymbol{K}$ is the absolute permeability; $k_{r\alpha}$, μ_α, and ρ_α are the relative permeability, dynamic viscosity, and mass density of phase α, respectively, with $\lambda_\alpha = k_{r\alpha}/\mu_\alpha$; p_α is the pressure of phase α; and $\boldsymbol{g}$ is the gravitational acceleration. The LBC method [31] was used to describe the phase viscosities. Relative permeabilities were evaluated based on Stone's model [32,33].

The total volume balance in the pressure equation is given by [34,35]:

$$\phi C_t \frac{\partial p_\alpha}{\partial t} + \sum_{i=1}^{n_c} \bar{V}_i \nabla . \left(\sum_\alpha c_\alpha x_{i,\alpha} v_\alpha + S_\alpha \boldsymbol{J_{i,\alpha}} \right) = \sum_{i=1}^{n_c} \bar{V}_i F_i \tag{5}$$

where C_t is the total compressibility and $\overline{V}_i$ is the total partial molar volume of component i.

The calculation of phase equilibrium was based on an initial guess from the stability analysis and the minimum of the Gibbs free energy. Equality of the fugacities of each component in the two hydrocarbon phases (oil and gas) implies:

$$f_{o,i}(T, p, x_{j,o}) = f_{g,i}(T, p, x_{j,g}), i = 2, ..n_c; j = 2, ..n_c - 1 \tag{6}$$

The indices i and j in the above equation start at two since the first component is considered to be the aqueous phase that is not allowed to dissolve in the hydrocarbon phases and vice versa. However, CO_2 dissolution is allowed in the aqueous phase. Note that Equation (5) assumes the same pressure in the gas and the oil phase and the curvature effect is assumed to be negligible in phase split calculations.

4. Examples

Four numerical examples are presented with different domain properties to study the effects of CO_2-enhanced viscosity and Fickian diffusion on oil recovery. The fourth numerical example is devoted to CO_2 sequestration in saline aquifers. Zero residual saturation of oil to CO_2 was considered and a 40% residual saturation of oil to water. Oil–water capillary pressure in the first two examples was calculated using Bensten and Anli's model [36]. Because the physics in every example is different, the number of elements varies between the examples. The mesh size in every example was chosen in a manner that guarantees numerical convergence. Further refinement in each mesh did not have a significant effect on the results.

4.1. Example 1: Homogeneous Medium

The first example is focused on the effect of CO_2 viscosity enhancement in a homogenous medium. A 1000×270 m^2 domain was discretized with 10,000 grids. Vertical injection and production wells were located at the left and right boundaries, respectively. Relevant data for the problem are given in Table 1, and the oil composition is shown in Table 2. The parameters for the use of the PR-EOS and CPA-EOS are provided in [37].

Table 1. Relevant data: Example 1.

Parameter	Value
Porosity	20%
Permeability	50 md
Temperature	333 K
Pressure	440 bar
Injection rate	0.1 PV/year
End-point relative permeability of oil to water, oil to gas, water, gas	1., 0.6, 0.2, 1.
Exponent for all phases	2.
Oil/water surface tension	50 dyne/cm

Table 2. Oil composition: Example 1.

Component	Overall Mole Fraction
CO_2	0.0824
N2 + C1	0.5166
C2	0.0707
C3	0.0487
C4–C5	0.0414
C6–C9	0.0656
C10–C14	0.0613
C15–C19	0.0371
C20+	0.0762

The effect of varying viscosification degree on oil recovery was considered. In WAG injection, CO_2 was injected for 0.5 PV followed by water for the same period; this was repeated for 2 cycles. In viscosified CO_2 injection, the viscosity varied from 2- to 10-fold. The oil density in reservoir conditions was 0.74 g/cm^3; the CO_2 density in reservoir conditions was 0.92 g/cm^3. Since CO_2 density is higher than that of the oil, CO_2 may segregate to the bottom.

Figure 1a,b shows the gas saturation from neat CO_2 injection and five viscosity enhancements (2-, 4-, 6-, 8-, and 10-fold viscosity enhancement with respect to the neat CO_2). All gas saturations in Figure 1 are at 30% PVI. Saturation plots show that viscosity enhancement delayed gas breakthrough by reducing the gas mobility. Sweep efficiency was improved with viscosity enhancement. Figure 2 shows the oil recovery. Two-fold viscosity enhancement increased the recovery by 20%. Increasing the viscosity by 10-fold led to a 40% improvement in recovery. It seems that a six-fold viscosity increase has a substantial effect on oil recovery improvement (the viscosity of the reservoir oil was 0.4 cp). A six-fold viscosification delayed breakthrough time by a factor of two compared to neat CO_2 injection. The WAG process in the homogenous media gave a recovery performance similar to that of neat CO_2 injection. In the next example, viscosified CO_2 injection is examined in a layered porous medium.

4.2. Example 2: Layered Media

This example considers a domain with nine alternating layers of 1 and 100 md starting with the high-permeability layer at the bottom. The domain size and relevant properties, including the oil composition and with the exception of permeability, were the same as in the previous example. Instead of injecting CO_2 first, water was injected first in the WAG process.

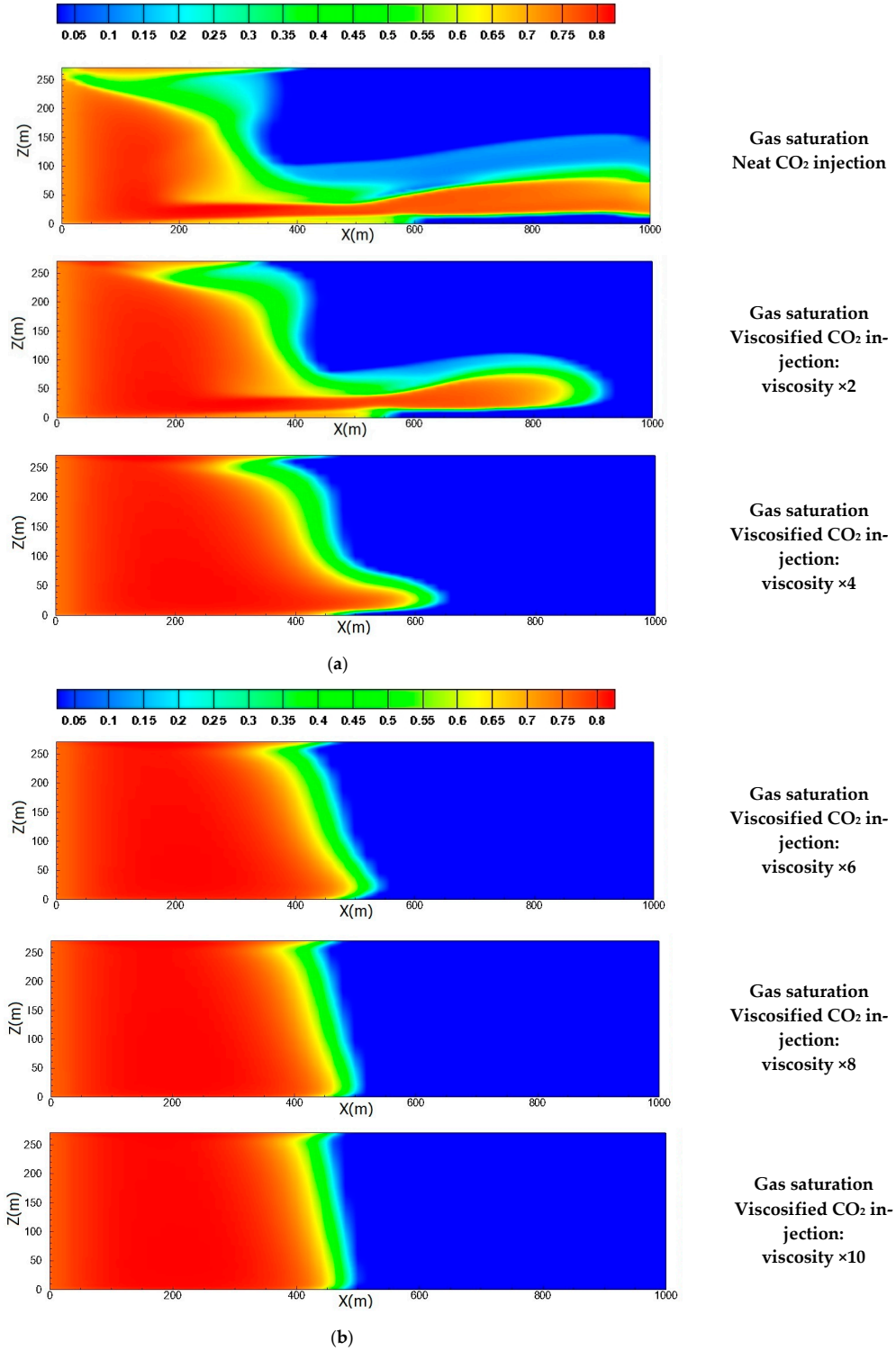

Figure 1. (**a**) Gas saturation at 30% PVI from viscosified CO_2 injection: Example 1, homogenous porous media. (**b**) Gas saturation at 30% PVI from viscosified CO_2 injection: Exampe 1, homogenous porous media.

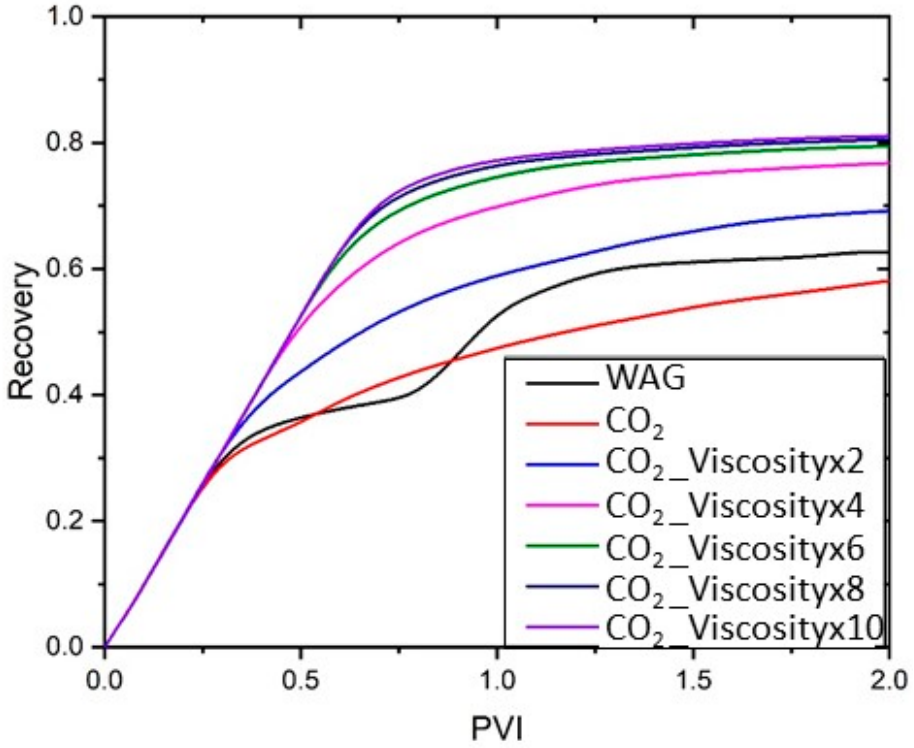

Figure 2. Oil recovery vs. PVI in viscosified CO_2, neat CO_2, and WAG injection: Example 1, homogenous media.

Different viscosity enhancement cases were simulated and compared were compared to neat CO_2 injection (from 2- to 10-fold enhanced viscosity). The high-permeability layers were the main flow conduits for the injected fluid; as a result, the oil from the low permeability layers was not much recovered. The contour plots of the gas saturation in different viscosity enhancements are shown in Figure 3a,b. Injected CO_2 mainly flowed through the high-permeability layers. As a result, the recovery in this example is lower than that in Example 1. Figure 4 shows the recovery plots for different viscosity enhancements. The high mobility of CO_2 and the layering of the domain with high contrast in permeability led to low recovery in neat CO_2 injection. Increasing the viscosity of the CO_2 led to high recovery from the more permeable layers. In the process, vaporized methane and light oil components dissolved in the CO_2. As a result, the CO_2-rich phase became lighter than the oil and therefore flowed on the top of the more permeable layers in neat CO_2 injection or when the viscosification was low. There was a significant effect of viscosification on cumulative recovery, which reached 50% at a 10-fold viscosity enhancement. As stated above, the WAG injection in this example was started by first injecting water instead of CO_2. This was done to prevent early breakthrough from the high-permeability layers. The results showed substantial recovery from low-permeability layers due to capillary crossflow in WAG injection.

The effect was not significant due to the very thick layers that have been assumed in this example.

4.3. Example 3: Fractured Media

Underground gas storage in fractured reservoirs helps store large amounts of gas. An integrated model for gas storage in fractured reservoirs is presented in [38]. This example expands into 3D fractured media. The same domain and oil properties are also used in Example 3. Other differences relate to the fracture permeability of 50 darcy (aperture of 0.5 mm). The domain dimensions are shown in Figure 5; the media was discretized with 60,000 grids. The size of the formation was very large.

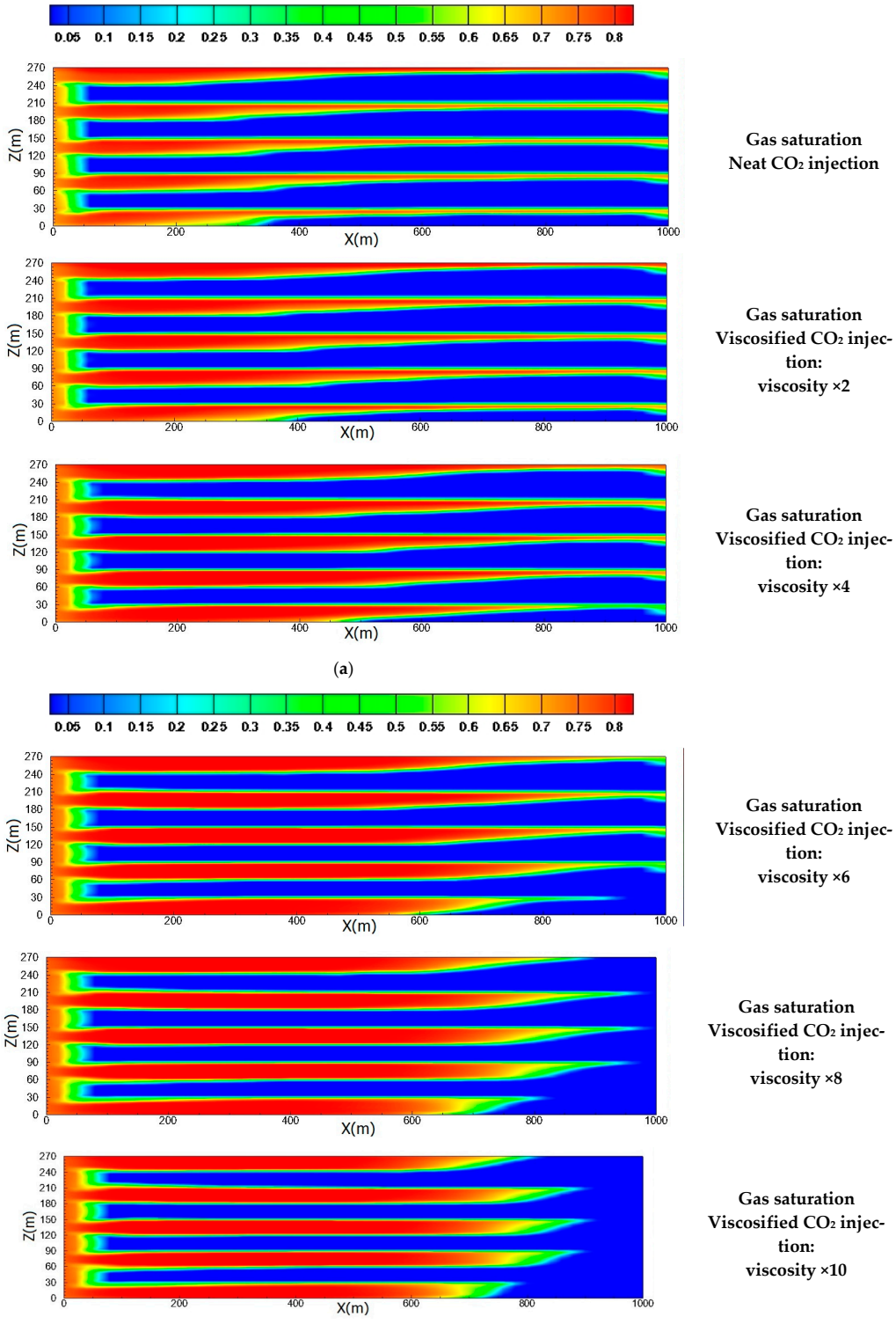

Figure 3. (**a**) Gas saturation at 30% PVI from neat and viscosified CO_2 injection: Example 2, layered media. (**b**) Gas saturation at 30% PVI from neat and viscosified CO_2 injection: Example 2, layered media.

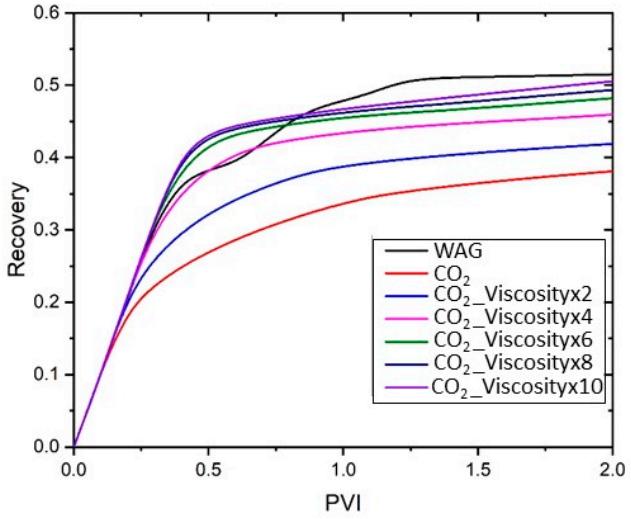

Figure 4. Oil recovery vs. PVI in viscosified CO_2, neat CO_2, and WAG injection: Example 2, layered media.

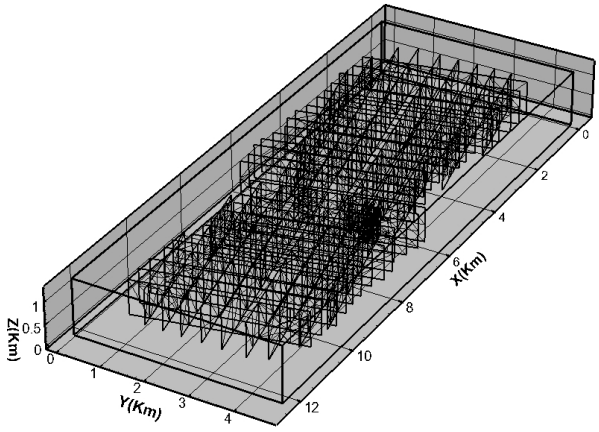

Figure 5. Domain dimensions and the fracture network: Example 3.

Injection and production wells were located at two diagonally opposite corners. The injection rate was 1% PV/year.

CO_2 injection in fractured media may give an early breakthrough due to high-permeability fractures. This is demonstrated in the contour plot of gas saturation at 10% PVI in neat CO_2 injection without viscosity enhancement (Figure 6). Fickian diffusion was not considered in the results in Figure 6. Viscosification may improve CO_2 injection performance and there may be a significant delay in breakthrough. Figure 7 depicts recovery performance. The breakthrough from neat CO_2 injection was around 10% PVI. At a 20-fold viscosity enhancement, the breakthrough time was doubled. There was also a significant increase in oil recovery performance from CO_2 viscosification. Further improvements to recovery required a viscosity enhancement greater than 20-fold.

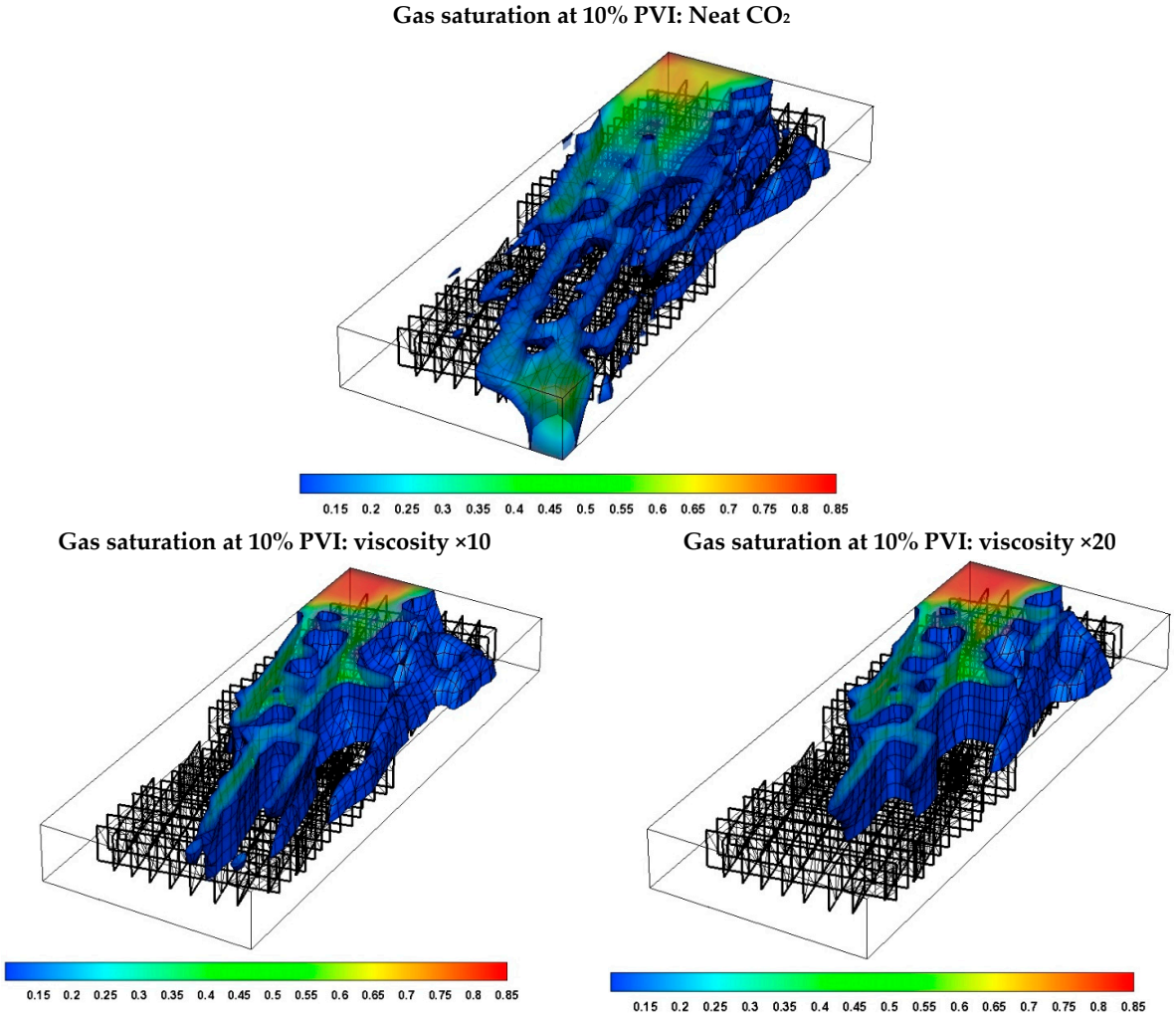

Figure 6. Gas saturation at 10% PVI from neat and viscosified CO_2 injection without Fickian diffusion: Example 3, fractured media.

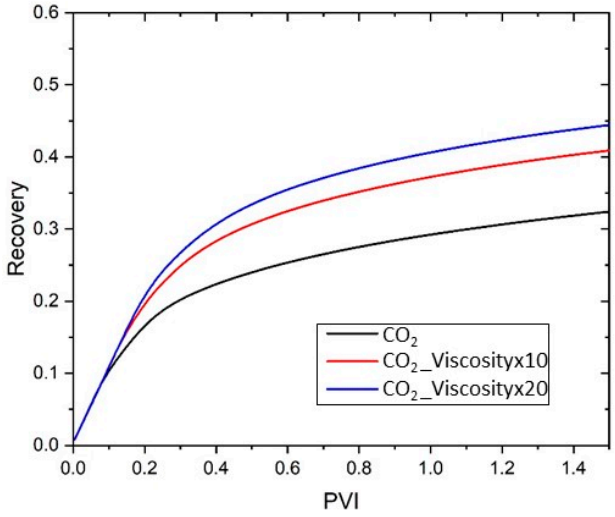

Figure 7. Oil recovery vs. PVI in neat CO_2, viscosified CO_2 and WAG injection, without Fickian diffusion: Example 3, fractured media.

The oil recovery results are shown in Figure 8; a 10-fold viscosity enhancement with Fickian diffusion gave about 47% recovery, whereas the recovery was about 38% with

neat CO_2 injection. A 20-fold increase in viscosity gave a recovery of more than 50%. The pronounced effect of Fickian diffusion is due to the large surface area of the rock matrix. In Figure 9, the gas saturation is shown at 10% PVI in neat and viscosified CO_2 injection.

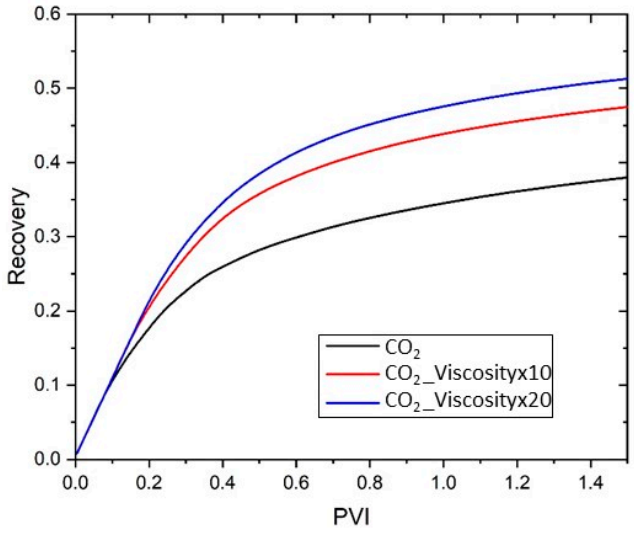

Figure 8. Oil recovery in different CO_2 viscosifications and WAG injection with Fickian diffusion: Example 3, fractured media.

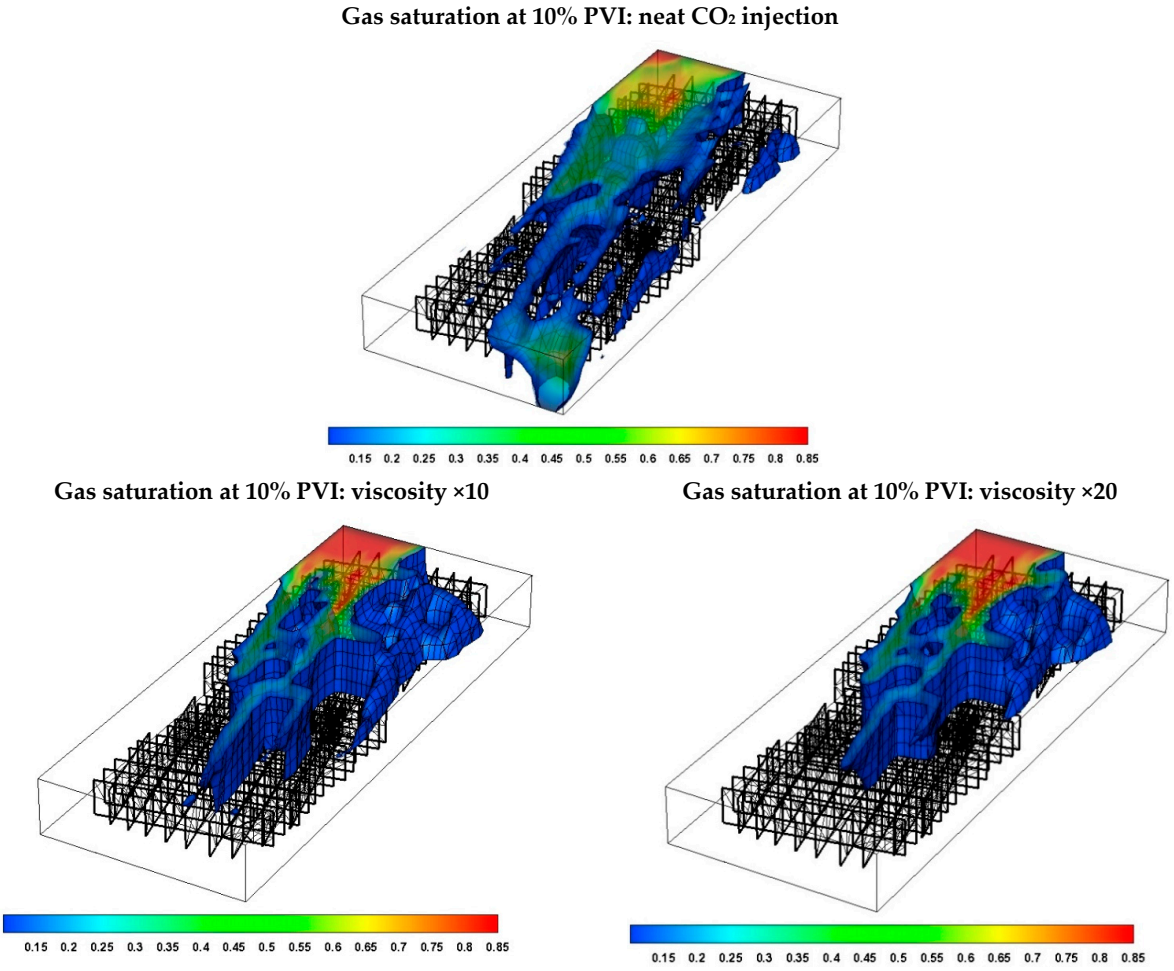

Figure 9. Gas saturation at 10% PVI in both neat and viscosified CO_2 injection with Fickian diffusion: Example 3, fractured media.

4.4. Example 4: CO_2 Sequestration

Carbon capture and storage is widely accepted as an effective strategy to mitigate anthropogenic CO_2 emissions. Containment of injected CO_2 is a critical part of the storage process. The extent to which the injected CO_2 can be immobilized by CO_2 viscosification was examined. A 2D aquifer domain of 100 × 100 m^2 was considered. The permeability was 1 darcy and porosity was 20%. The domain was discretized with 10,000 quadrangles. The residual saturation of water was 30%; the endpoints were one and the exponents were two for both water and CO_2. The injection of CO_2 at the middle of the top boundary of the domain over injection lengths of 1 m and 5 m was investigated. The injection of neat CO_2 is compared to the five-fold viscosity enhancement. The injection rate was 0.15% PV/year. The initial pressure at the bottom was 100 bar, and the temperature was 350 K.

Figure 10 shows the CO_2 mole fraction at 0.6 years (neat and viscosified CO_2) for the 1 m injection length at the middle of the top boundary.

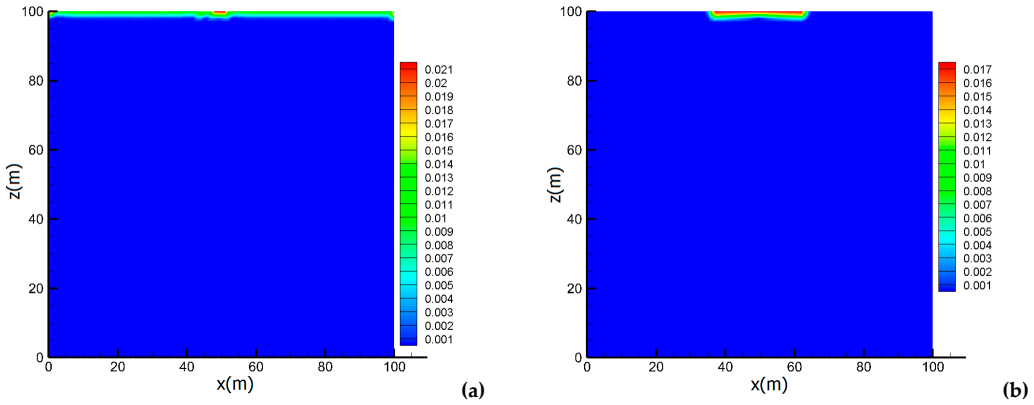

Figure 10. CO_2 overall mole fraction at 0.6 years of injection, neat CO_2 (**a**) and viscosified CO_2, 5-fold (**b**): Example 4, 1 m injection length.

The pressure at the injection well at 0.6 years of injection increased to 105 bar from viscosified CO_2 and to 164 bar from neat CO_2 injection. At 2 years of injection the pressure at the injector location was 124 bar (viscosified) and 188 bar (neat) CO_2 injection. At 20 years the pressure was 303 bar (viscosified) and 377 bar (neat). Figure 11 shows the CO_2 overall mole fraction at 20 years of injection.

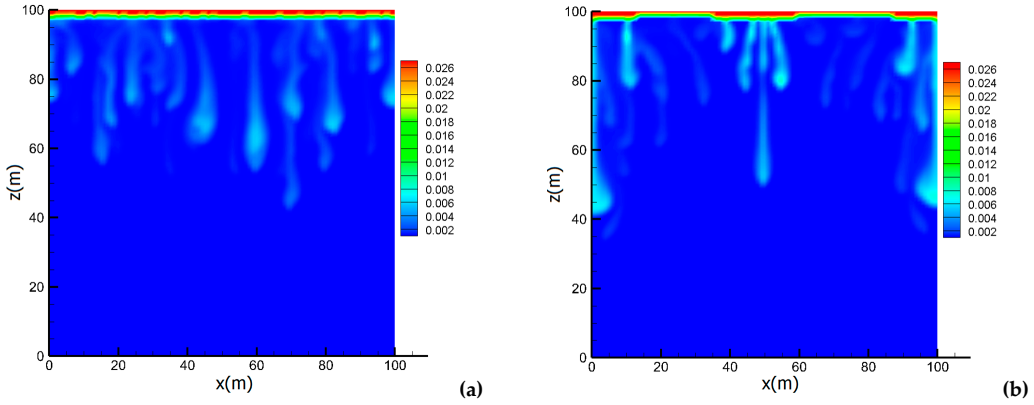

Figure 11. CO_2 overall mole fraction at 20 years of injection, neat CO_2 (**a**) and viscosified CO_2, 5-fold (**b**): Example 4, 1 m injection length.

To evaluate the effect of a large injection length, the simulation considered the effect of a 5 m injection length symmetrically located at the top middle boundary. A large injection length leads to lower pressure buildup. In the neat CO_2 injection, the pressure at the injector was 103 bar, and in the viscosified CO_2 injection, the pressure was 102 bar at 0.6 years of

injection. In Figure 12, the CO_2 overall mole fraction is shown at 20 years of injection with the 5 m injection length at the top.

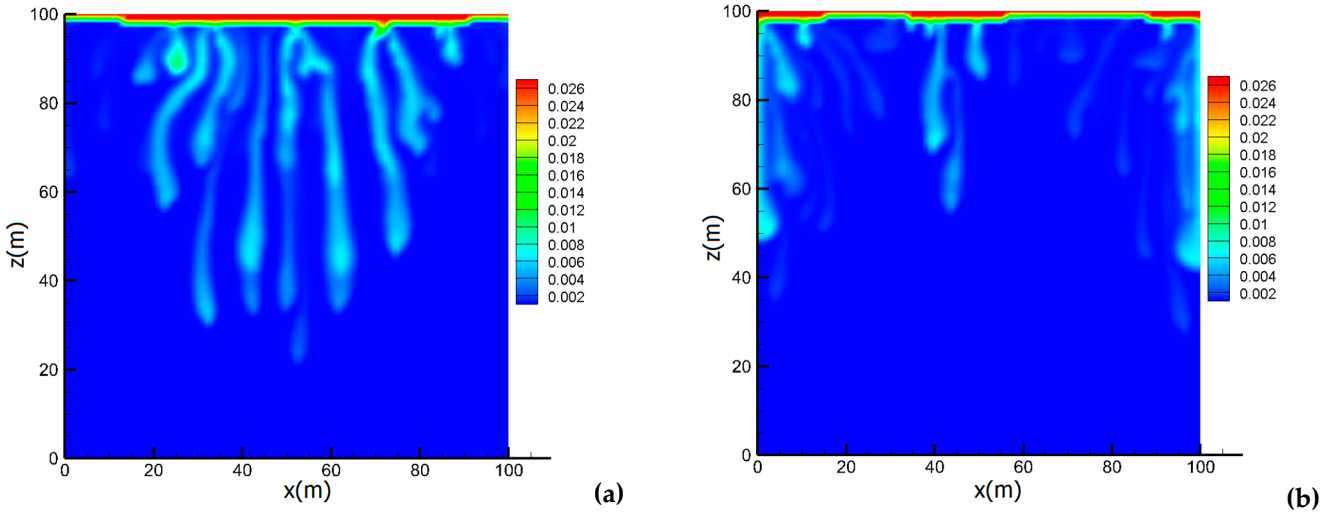

Figure 12. CO_2 overall mole fraction at 20 years of injection, neat CO_2 (**a**) and viscosified CO_2, 5-fold (**b**): Example 4, 5 m injection length.

Due to the greater injection length, the pressure buildup in the neat CO_2 injection was 330 bar. In the viscosified CO_2 injection, the pressure at the injector was 303 bar. The distribution of the overall mole fraction of CO_2 in the water phase showed a higher concentration near the middle region in the neat CO_2 injection. The results indicated that viscosification for the small injection length had a higher effect on the mitigation of pressure increase from CO_2 sequestration in saline aquifers.

5. Statistical Analysis

A detailed statistical analysis is presented in this section. The aim is to quantify the effect of injection rate, permeability, and a two-fold viscosity enhancement on the position of the injected CO_2 front as a function of PVI. The more the front is retarded, the more the sweeping efficiency is improved. This study considered the average position of the CO_2 front to be a dependent variable of injection rate, permeability, and viscosity enhancement. In this study, a regression model was developed to predict the position of the CO_2 front based on a combination of 12 independent simulations. The 12 simulations were divided into two groups, each of which consisted of 6 independent simulations, the first group without viscosity enhancement and the second group with a doubling of the viscosity of the injected CO_2. Within each subgroup (six independent simulations) three different injection rates were considered: 0.05, 0.1, and 0.2 PV/year. With each injection rate a separate simulation was considered on a domain with permeability values of 10 and 50 md. During each of the independent simulations, the average position of the CO_2 front at a different PVI was recorded. A total of 1300 data points were obtained, of which 900 data points were used to develop the regression model. The independent variables have different dimensions; therefore, a standardization was applied with respect to their average value and the respective standard deviation. Table 3 shows the regression coefficients for the three independent (standardized) variables: injection rate, permeability, and viscosity enhancement. As shown in Table 3, the effect of viscosity enhancement on retarding the CO_2 front (and as a result on improving sweeping efficiency) was almost double the injection rate effect. The effect of the latter (injection rate) was around 18 times more important to front displacement compared to the effect of permeability. As expected, permeability had a positive regression weight. That is, the higher the permeability, the faster the front travels in the reservoir. Figure 13 shows the predicted front position in the reservoir (in meters) as a function of the actual front position (the one obtained from the

simulation). The same plot shows the exact solution (that is, if the model is 100% accurate). The results show that the model can give an accurate predicted front position compared to the exact front position obtained from the simulations; however, the model is more accurate in predicting the front in the enhanced viscosity compared to the unaltered viscosity. This is because without viscosity enhancement, CO_2 mobility is much higher, and therefore the front displacement is much faster. This makes the prediction error higher. Figure 14 shows the probability distribution function (PDF) for the difference in the front position between the predicted and actual values. The PDF plot shows that the difference between the predicted and actual values was concentrated around zero, indicating the accuracy of the regression model.

Table 3. Weights of standardized independent variables.

Standardized Variable	Weight Value
Permeability	1.54
Injection rate	−28.98
Viscosity enhancement	−55.63

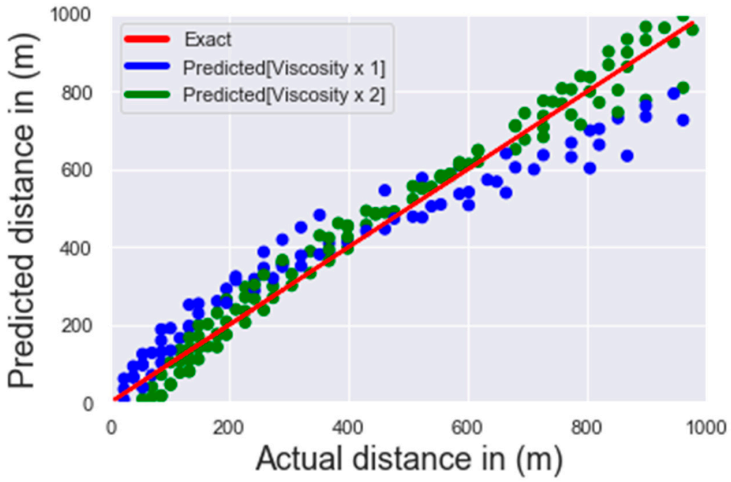

Figure 13. Predicted front position as a function of actual distance with and without viscosity enhancement; the red line represents the exact solution (assuming the model is 100% accurate) and the dots represent the model-predicted front position.

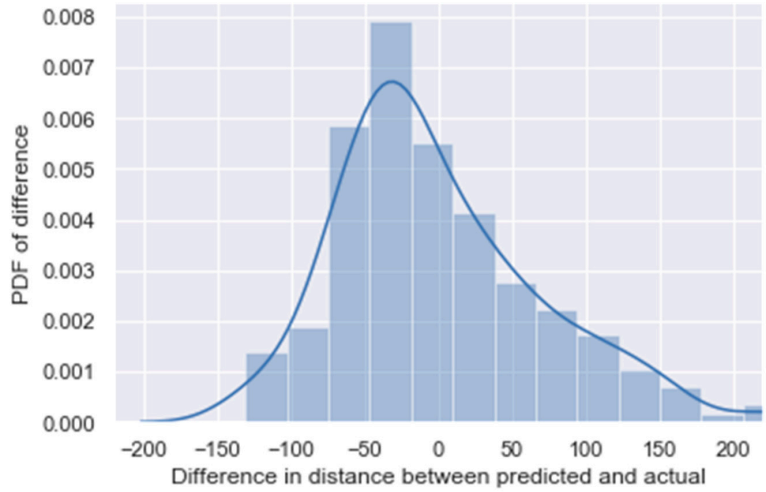

Figure 14. Probability distribution function of the difference in front position between the predicted and actual values.

6. Concluding Remarks

Viscosified CO_2 oligomer hydrocarbons have recently advanced in effectiveness. A major element of effectiveness of new molecules is negligible adsorption. Another observed side effect of viscosification is a reduction in residual water saturation. In the simulations presented in this work, the change in residual saturation from viscosified CO_2 has not been included. Nevertheless, a significant increase in the breakthrough time was observed.

This work centers around an investigation of the degree of viscosification that will increase oil recovery performance in unfractured and fractured media. In CO_2 sequestration, the viscosity of reservoir brine, especially at high reservoir temperature conditions, may require an increase by a factor of five to six. The mobility can then be improved significantly. In oil formations, depending on layering and on the extent of the fractures, a viscosity increase of CO_2 may be several times this or higher.

The critical element in subsurface storge and use of CO_2 is mobility control. In oil recovery applications, the outcome is a delay in breakthrough time. In CO_2 sequestration, the increase in dissolution trapping and the lowering of the pressure increase contribute to safer conditions.

Higher-order discretization schemes have been used in composition calculation and mixed finite element in flux calculation for high accuracy. In future work, more detailed simulations with more accurate relative permeability and capillary pressure functions can be used to cover the effects of formation heterogeneity, layering, and fractures.

The use of viscosified CO_2 is expected to be the method of choice due to the simplicity of the process compared to alternatives, its effectiveness, and its compatibility with current trends in environmental stewardship.

Funding: This research received no external funding.

Institutional Review Board Statement: Not applicable.

Informed Consent Statement: Not applicable.

Data Availability Statement: Not applicable.

Conflicts of Interest: The author declare no conflict of interest.

References

1. Lemaire, P.C.; Alenzi, A.; Lee, J.J.; Beckman, E.J.; Enick, R.M. Thickening CO_2 with Direct Thickeners, CO_2-in-Oil Emulsions, or Nanoparticle Dispersions: Literature Review and Experimental Validation. *Energy Fuels* **2021**, *35*, 8510–8540. [CrossRef]
2. Wu, Z.; Huiqing, L.; Wang, X.; Zhang, Z. Emulsification and improved oil recovery with viscosity reducer during steam injection process for heavy oil. *J. Ind. Eng. Chem.* **2017**, *61*, 348–355. [CrossRef]
3. Green, D.W.; Willhite, G.P. *Enhanced Oil Recovery: Society of Petroleum Engineers Textbook Series, V.6*; SPE: Richardson, TX, USA, 1998.
4. Lake, L.W. *Enhanced Oil Recovery: Upper Saddle River*; Prentice Hall: Hoboken, NJ, USA, 1989.
5. Torabi, F.; Jamaloei, B.Y.; Zarivnyy, O.; Paquin, B.A.; Rumpel, N.J.; Wilton, R.R. Effect of Oil Viscosity, Permeability and Injection Rate on Performance of Waterflooding, CO_2 Flooding and WAG Processes on Recovery of Heavy Oils. In Proceedings of the Canadian Unconventional Resources and International Petroleum Conference, Calgary, AB, Canada, 19–21 October 2010. [CrossRef]
6. Jian, G.; Zhang, L.; Da, C.; Puerto, M.; Johnston, K.P.; Biswal, S.L.; Hirasaki, G.J. Evaluating the Transport Behavior of CO_2 Foam in the Presence of Crude Oil under High-Temperature and High-Salinity Conditions for Carbonate Reservoirs. *Energy Fuels* **2019**, *33*, 6038–6047. [CrossRef]
7. Jian, G.; Fernandez, C.A.; Puerto, M.; Sarathi, R.; Bonneville, A.; Biswal, S.L. Advances and challenges in CO_2 foam technologies for enhanced oil recovery in carbonate reservoirs. *J. Pet. Sci. Eng.* **2021**, *202*, 108447. [CrossRef]
8. Bond, D.C.; Holbrook, O.C. Gas Drive Oil Recovery Process. U.S. Patent 2,866,507,12,24, 1958.
9. Fried, A.N. *The Foam Drive Process for Increasing the Recovery of Oil*; re. inv 5866; US Bureau of Mines: Washington, DC, USA, 1961.
10. Yang, S.H.; Reed, R.L. Mobility Control Using CO_2 Forms. In Proceedings of the SPE Annual Technical Conference and Exhibition, San Antonio, TX, USA, 8–11 October 1989. [CrossRef]
11. Khulman, M.I. Visualizing the Effect of Light Oil on CO_2 Foams. *J. Pet. Technol.* **1990**, *42*, 902–908.
12. Manlowe, D.J.; Radke, C.J. A Pore-Level Investigation of Foam/Oil Interactions in Porous Media. *Soc. Pet. Eng.* **1990**, *5*, 495–502. [CrossRef]

13. Nikolov, A.D.; Wasan, D.T.; Huang, D.W.; Edwards, D.A. The Effect of Oil on Foam Stability: Mechanisms and Implications for Oil Displacement by Foam in Porous media. In Proceedings of the 61st ATCE of SPE, New Orleans, LA, USA, 5 October 1986.
14. Bernard, G.G.; Holm, L. Effect of Foam on Permeability of Porous Media to Gas. *Soc. Pet. Eng. J.* **1965**, *4*, 267. [CrossRef]
15. Rogers, J.D.; Grigg, R.B. A Literature Analysis of the WAG Injectivity Abnormalities in the CO_2 Process. In Proceedings of the SPE/DOE Improved Oil Recovery Symposium, Tulsa, OK, USA, 3–5 April 2000. [CrossRef]
16. Gallo, G.; Erdmann, E. Simulation of Viscosity Enhanced CO_2 Nanofluid Alternating Gas in Light Oil Reservoirs. In Proceedings of the SPE Latin America and Caribbean Petroleum Engineering Conference, Buenos Aires, Argentina, 17–19 May 2017. [CrossRef]
17. Bae, J.H.; Irani, C.A. A Laboratory Investigation of Viscosified CO_2 Process. *Soc. Pet. Eng.* **1993**, *1*, 166–171. [CrossRef]
18. Xu, J.; Enick, R.M. Thickening Carbon Dioxide with the Fluoroacrylate-Styrene Copolymer. In Proceedings of the SPE Annual Technical Conference and Exhibition, New Orleans, LA, USA, 30 September–3 October 2001. [CrossRef]
19. Huang, Z.; Xu, S.J.; Kilic, R.M. Enhancement of Viscosity of Carbon Dioxide Using Styrene/Fluoroacrylate Copolymers. *Macromolecules* **2000**, *33*, 5437–5442. [CrossRef]
20. Zaberi, H.A.; Lee, J.J.; Enick, R.M.; Beckman, E.J.; Cummings, S.D.; Dailey, C.; Vasilache, M. An experimental feasibility study on the use of CO_2-soluble polyfluoroacrylates for CO_2 mobility and conformance control applications. *J. Pet. Sci. Eng.* **2020**, *184*, 106556. [CrossRef]
21. Kilic, S.; Enick, R.M.; Beckman, E.J. Fluoroacrylate-Aromatic Acrylate Copolymers for Viscosity Enhancement of CarbonDioxide. *J. Supercrit. Fluids* **2019**, *146*, 38–46. [CrossRef]
22. Peng, D.Y.; Robinson, D.B. A new two-constant equation of state. *Ind. Eng. Chem. Fundam.* **1976**, *15*, 59–64. [CrossRef]
23. Kruger, F.; Kontogeorgis, G.M.; von Solms, N. New association schemes for mono-ethylene glycol: Cubic-Plus-Association parameterization and uncertainty analysis. *Fluid Phase Equilibria* **2018**, *458*, 211–233. [CrossRef]
24. Tian, Y.; Zhang, C.; Lei, Z.; Yin, X.; Kazemi, H.; Wu, Y.-S. An improved multicomponent diffusion model for compositional simulation of fractured unconventional reservoirs. *Soc. Pet. Eng.* **2021**, *26*, 3316–3341. [CrossRef]
25. Zidane, A.; Younes, A.; Huggenberger, P.; Zechner, E. The Henry semianalytical solution for saltwater intrusion with reduced dispersion. *Water Resour. Res.* **2012**, *48*. [CrossRef]
26. Zidane, A.; Zechner, E.; Huggenberger, P.; Younes, A. Simulation of rock salt dissolution and its impact on land subsidence. *Hydrol. Earth Syst. Sci.* **2014**, *18*, 2177–2189. [CrossRef]
27. Younes, A.; Makradi, A.; Zidane, A.; Shao, Q.; Bouhala, L. A combination of Crouzeix-Raviart, Discontinuous Galerkin and MPFA methods for buoyancy-driven flows. *Int. J. Numer. Methods Heat Fluid Flow* **2014**, *24*, 735–759. [CrossRef]
28. Younes, A.; Konz, M.; Fahs, M.; Zidane, A.; Huggenberger, P. Modelling variable density flow problems in heterogeneous porous media using the method of lines and advanced spatial discretization methods. *Math. Comput. Simul.* **2011**, *81*, 2346–2355. [CrossRef]
29. Zechner, E.; Zidane, A.; Younes, A.; Huggenberger, P. Simulation of high-contrast density driven transport. SWIM 22, 2014, 247–250. Available online: https://www.semanticscholar.org/paper/Simulation-of-high-contrast-densitiy-driven-at-Zechner-Zidane/20c2056c19e24765349d20a2a6df1258d6ae8a1b (accessed on 23 April 2023).
30. Zidane, A. Modeling two-phase flow in heterogeneous porous media: Part 1, the case of low interfacial tension. *Authorea* **2023**. [CrossRef]
31. Lohrenz, J.; Bray, B.G.; Clark, C.R. Calculating Viscosities of Reservoir Fluids from Their Compositions. *J. Pet. Technol.* **1964**, *16*, 1171–1176. [CrossRef]
32. Stone, H. Estimation of Three-Phase Relative Permeability and Residual Oil Data. *J. Can. Pet. Technol.* **1973**, *12*, 53–61. [CrossRef]
33. Stone, H. Probability Model for Estimating Three-Phase Relative Permeability. *J. Pet. Technol.* **1970**, *22*, 214–218. [CrossRef]
34. Ács, G.; Doleschall, S.; Farkas, E. General Purpose Compositional Model. *Soc. Pet. Eng. J.* **1985**, *25*, 543–553. [CrossRef]
35. Watts, J.W. A Compositional Formulation of the Pressure and Saturation Equations. *SPE Reserv. Eng.* **1986**, *1*, 243–252. [CrossRef]
36. Bensten, R.G.; Anli, J. A New Displacement Capillary Pressure Model. *J. Cdn. Pet. Tech.* **1976**, *15*, 75–79.
37. Zidane, A. Multiphase Unified Flash Analysis and Stability Algorithm (MUFASA): An Open-Source Software. *arXiv* **2022**, arXiv:2211.15373. [CrossRef]
38. Xue, W.; Wang, Y.; Chen, Z.; Liu, H. An integrated model with stable numerical methods for fractured underground gas storage. *J. Clean. Prod.* **2023**, *393*, 136268. [CrossRef]